PHYSICAL REVIEW D **85,** 076002 (2012)

Nonet meson properties in Nambu-Jona-Lasinio model with dimensional regularization at finite temperature and chemical potential

T. Inagaki
Information Media Center, Hiroshima University, Higashi-Hiroshima, Hiroshima 739-8521, Japan

D. Kimura
Faculty of Education, Hiroshima University, Higashi-Hiroshima, Hiroshima 739-8524, Japan

H. Kohyama
Department of Physics, Chung-Yuan Christian University, Chung-Li 32023, Taiwan

A. Kvinikhidze
A. Razmadze Mathematical Institute of Georgian Academy of Sciences, M. Alexidze Str. 1, 380093 Tbilisi, Georgia
(Received 27 October 2011; published 4 April 2012)

The nonet meson properties are studied in the Nambu-Jona-Lasinio model at finite temperature and chemical potential using dimensional regularization. This study leads to the reasonable description which is mainly similar to one obtained in the model with the cutoff regularization. However, remarkable differences between the two regularizations are observed in the behavior of the chiral phase transition at finite chemical potential.

DOI: 10.1103/PhysRevD.85.076002 PACS numbers: 11.10.Wx, 11.30.Qc, 12.39.−x

I. INTRODUCTION

Mesons are composed of quarks, interacting with each other through the exchange of gluons. Under the low temperature and density conditions, quarks are confined in hadrons and therefore are not observed as free particles, which makes their investigation challenging. The phenomenon of confinement is closely related to the dynamical chiral symmetry breaking. While the chiral symmetry broken in vacuum is expected to be restored at high temperature and density, it is also expected that the properties of mesons are affected by this chiral phase transition. Thus the investigation of meson properties at finite temperature and density is an important part of hadron physics.

Such investigation unfortunately cannot be pursued directly in the framework of quantum chromodynamics (QCD), the ultimate theory of strong interaction, due to its large coupling constant at low-energy scale and thereby the necessity of dealing nonperturbatively with its notoriously complicated structure. The investigations are usually performed by using the effective models which share the same symmetry properties with QCD such as the Nambu-Jona-Lasinio (NJL) model [1], the linear sigma model [2], or by using the discretized version of QCD, i.e., the lattice QCD [3].

We employ, in this paper, the NJL model to study the nonet meson properties (for reviews on the model, see e.g., [4–7]). It is not renormalizable therefore one has to introduce the regularization procedure to handle the divergences appearing in loop integrals. There are several regularization schemes: the three- and four-momentum cutoff regularization, the dimensional regularization, the Pauli-Villars methods, and so on. We shall use the dimensional regularization (DR) in this paper. In the DR method the divergent fermion loop integrals which are the functions of the space-time dimensions are regularized by applying an analytic continuation in the dimensions variable. Many works are devoted to the studies based on it (see e.g., [8–12]).

We believe that a regularization procedure is an important *dynamical* part of the NJL model, it determines the size and the shape of the interaction between quarks, which otherwise is point-like in the traditionally used leading-order approximation of the $1/N_c$ expansion. That is why it is important to chose a proper regularization. Dimensional and cutoff regularizations can be considered as corresponding to the same size but different shape of the interaction. The fact that some physical results depend on the regularization may imply that the corresponding physics is sensitive (probes) not only to the size of the interaction but to its shape as well. If so the regularization-dependent properties would be determined by higher energy (shorter distances) than those which do not depend on the regularization procedure.

The purpose of this paper is to study the nonet meson properties such as masses and decay constants in the three-flavor NJL model with the DR at finite temperature T and chemical potential μ. To this end one has to first determine the model parameters so that the model describes the physical ingredients properly. This has been done in the paper [13], where the present authors have found that the various parameter sets reproduce the meson properties nicely at $T = 0$ and $\mu = 0$. As our goal is to study meson properties at finite T and μ, the paper is the straightforward extension of the previous work [13].

This paper is organized as follows: In Sec. II, the three-flavor NJL model and its parameters are introduced. In Sec. III we discuss the constituent quark masses and chiral condensates which are derived through solving the gap equations. The results on the meson properties and topological susceptibility are shown in Sec. IV. Section V is devoted to the discussion of the critical temperature. Summary and discussions are given in Sec. VI. The required calculations of the chiral condensates and meson properties are aligned in Appendix A and B. The fitted parameters except those in Sec. II are shown in Appendix C.

II. NJL MODEL WITH $U_A(1)$ ANOMALY

A. The model

The Lagrangian of our three-flavor NJL model is

$$\mathcal{L}_{\rm NJL} = \sum_{i,j} \bar{q}_i (i\not{\partial} - \hat{m})_{ij} q_j + \mathcal{L}_4 + \mathcal{L}_6, \tag{1}$$

where

$$\mathcal{L}_4 = G \sum_{a=0}^{8} \left[\left(\sum_{i,j} \bar{q}_i \lambda_a q_j \right)^2 + \left(\sum_{i,j} \bar{q}_i i\gamma_5 \lambda_a q_j \right)^2 \right], \tag{2}$$

$$\mathcal{L}_6 = -K[\det \bar{q}_i (1-\gamma_5) q_j + \text{H.c.}]. \tag{3}$$

Here the subscripts i, j represent the flavor indices, $\hat{m}$ is the current quark mass matrix diag (m_u, m_d, m_s), and λ_a are the Gell-Mann matrices in flavor space with $\lambda_0 = \sqrt{2/3} \cdot \mathbf{1}$. $\mathcal{L}_4$ and $\mathcal{L}_6$ are the four- and six-fermion interactions with the effective coupling constants G and K. $\mathcal{L}_6$ is introduced to break the $U_A(1)$ symmetry which is not realized in the real world. The six-quark vertex in the determinant form was first discussed by Kobayashi and Maskawa [14] and later derived by 't Hooft as an instanton-induced quark interaction [15], so this vertex is called Kobayashi-Maskawa-'t Hooft term.

To study the thermal system we evaluate the thermodynamic potential $\Omega = -\ln Z/(V\beta)$, with the partition function Z, the volume of the system V, and the inverse temperature $\beta(\equiv 1/T)$. Here we use the imaginary time formalism to treat the system at finite T and μ. Applying the mean-field approximation in the DR scheme, we obtain the following thermodynamic potential:

$$\begin{aligned}\Omega = {} & 2G(\phi_u^2 + \phi_d^2 + \phi_s^2) - 4K\phi_u\phi_d\phi_s \\ & - \frac{2^{D/2} N_c}{2} \int \frac{d^{D-1}p}{(2\pi)^{D-1}} [E_u + E_d + E_s] \\ & - \frac{2^{D/2} N_c}{2} T \int \frac{d^{D-1}p}{(2\pi)^{D-1}} \sum_{i,\pm} \ln[1 + e^{-\beta E_i^{\pm}}],\end{aligned} \tag{4}$$

where $\phi_i \equiv \langle \bar{i}i \rangle$ represent the chiral condensates and $N_c(=3)$ is the number of colors. $E_i = \sqrt{p^2 + m_i^{*2}}$ is the energy of the quasiparticle, and $E_i^{\pm} = E_i \pm \mu$, with the constituent quark masses m_i^* and a chemical potential μ. For simplicity, we take $\mu = \mu_u = \mu_d = \mu_s$. In this scheme we regularize the divergent integrals by performing the analytic continuation of the space-time dimension D to a value less than four, then the integral can be written as

$$\int \frac{d^{D-1}p}{(2\pi)^{D-1}} = \frac{2(4\pi)^{-(D-1)/2}}{\Gamma[(D-1)/2]} M_0^{4-D} \int_0^\infty dp p^{D-2}, \tag{5}$$

where M_0 is a renormalization scale. One can switch to cutoff regularization through the replacement

$$\int \frac{d^{D-1}p}{(2\pi)^{D-1}} \to \frac{1}{2\pi^2} \int_0^\Lambda dp p^2. \tag{6}$$

The chiral condensates ϕ_i which are the order parameters of the model are evaluated through solving the gap equations, $\partial\Omega/\partial\phi_i = 0$. After some algebra, one arrives at the following self-consistent equations:

$$m_i^* = m_i - 4G\phi_i + 2K\phi_j\phi_k, \qquad (i \neq j \neq k), \tag{7}$$

where

$$\phi_i = \frac{1}{\beta} \sum_{-\infty}^{\infty} \int \frac{d^{D-1}p}{(2\pi)^{D-1}} \, \text{tr} S^i(p), \tag{8}$$

$$S^i(p) = \frac{1}{\boldsymbol{p}\cdot\boldsymbol{\gamma} - (\omega_n - i\mu)\gamma_4 + m_i^* - i\epsilon},$$

with $\omega_n = (\pi/\beta)(2n+1)$, $(n = 0, \pm 1, \pm 2, \cdots)$. The "tr" stands for the trace in spinor and color indices. The explicit form of the integral is presented in the Appendix A.

To evaluate meson properties, one needs to carry out further calculations as discussed in [13] where only the case of $T, \mu = 0$ is presented. We carry out the corresponding calculations for the case of finite T and μ in the Appendix B.

B. Topological susceptibility

The topological susceptibility χ has a special importance because we use it to fix the model parameters in this letter. It is given by the correlation function between the topological charge densities $Q(x)$ at different points [16],

$$\chi = \int d^4x \langle 0|TQ(x)Q(0)|0\rangle_{\text{connected}}, \tag{9}$$

where the charge density is defined as

$$Q(x) \equiv \frac{g^2}{32\pi^2} F^a_{\mu\nu} \tilde{F}^{a\mu\nu} = 2K \, \text{Im}[\det \bar{q}(1-\gamma_5) q], \tag{10}$$

with g, the QCD coupling constant, and $F^a_{\mu\nu}$, the gluon field strength. The explicit form of χ is,

$$\chi = -\frac{4K^2}{M_0^{D-4}}\phi_u^2\Bigg[\phi_u\phi_s\left(\frac{2\phi_s}{m_u^*}+\frac{\phi_u}{m_s^*}\right) - \left\{\frac{1}{\sqrt{6}}(2\phi_s+\phi_u)(\Pi_{00}(0),\Pi_{08}(0)) + \frac{1}{\sqrt{3}}(\phi_s-\phi_u)(\Pi_{08}(0),\Pi_{88}(0))\right\}\mathbf{\Delta}^+(0) \times \left\{\frac{1}{\sqrt{6}}(2\phi_s+\phi_u)\begin{pmatrix}\Pi_{00}(0)\\ \Pi_{08}(0)\end{pmatrix} + \frac{1}{\sqrt{3}}(\phi_s-\phi_u)\begin{pmatrix}\Pi_{08}(0)\\ \Pi_{88}(0)\end{pmatrix}\right\}\Bigg]. \quad (11)$$

The forms of Π_{00}, Π_{08}, Π_{88}, and $\mathbf{\Delta}^+$ are shown by Eqs. (B22), (B24), (B23), and (B16) in Appendix B 3. After solving the gap equations, one can numerically calculate this quantity by inserting the values of ϕ_i and m_i^*.

C. Model parameters

In the DR, the three-flavor NJL model has seven parameters:

(i) current quark masses m_u, m_d, m_s
(ii) four-point coupling G
(iii) six-point coupling K
(iv) dimensions D
(v) renormalization scale M_0.

Since the mass difference between m_u and m_d is small as compared to one between m_s and m_u (or m_d), we take the isospin limit, $m_d = m_u$, and test several values, $m_u = 3, 4, 5, 5.5, 6$ MeV. To fix the other parameters, we usually employ the following physical observables [17]:

$$m_\pi = 138\ \text{MeV}, \qquad f_\pi = 92\ \text{MeV}, \qquad m_{\rm K} = 495\ \text{MeV}, \qquad m_{\eta'} = 958\ \text{MeV}. \quad (12)$$

One more physical quantity is needed to fix all seven above listed parameters. Possible candidates are the alternative meson properties such as the η meson mass, m_η, topological susceptibility, χ, kaon decay constant, $f_{\rm K}$, etc. We choose the following three cases:

Case m_η $\quad m_\pi, m_{\rm K}, f_\pi, m_{\eta'}, m_\eta = 548$ MeV
Case χ_{170} $\quad m_\pi, m_{\rm K}, f_\pi, m_{\eta'}, \chi^{1/4} = 170$ MeV
Case χ_{179} $\quad m_\pi, m_{\rm K}, f_\pi, m_{\eta'}, \chi^{1/4} = 179$ MeV.

TABLE I. Case $m_\eta^{\rm LD}$.

m_u	m_s	G	K	M_0	D
3.0	84.9	−0.0195	9.02×10^{-7}	118	2.29
4.0	118	−0.0174	9.17×10^{-7}	113	2.38
5.0	156	−0.0162	9.49×10^{-7}	108	2.47

TABLE II. Case m_η.

m_u	m_s	G	K	M_0	D
3.0	79.0	−0.0130	2.29×10^{-7}	107	2.37
4.0	106	−0.007 48	8.26×10^{-8}	92.0	2.52
5.0	134	−0.003 57	1.99×10^{-8}	73.2	2.69
5.5	147	−0.002 31	8.40×10^{-9}	62.4	2.77
6.0	162	−0.001 42	3.23×10^{-9}	50.9	2.87

TABLE III. Case χ_{170}.

m_u	m_s	G	K	M_0	D
3.0	77.1	−0.0168	2.23×10^{-7}	120	2.28
4.0	106	−0.0143	2.11×10^{-7}	116	2.36
5.0	134	−0.0119	1.80×10^{-7}	112	2.43
5.5	150	−0.0109	1.62×10^{-7}	110	2.47
6.0	166	−0.009 92	1.48×10^{-7}	109	2.50

TABLE IV. Case cutoff.

m_u	m_s	$G\Lambda^2$	$K\Lambda^5$	Λ
3.0	89.5	1.55	8.34	960
4.0	110	1.60	8.38	797
5.0	128	1.71	8.77	682
5.5	136	1.81	9.17	630
5.87	139	2.09	10.1	580

As mentioned in the introduction, the parameters are fixed at $T, \mu = 0$ in [13]; we show the sets of them in Tables I, II, and III. In the Case m_η, there exist two sets of parameters, and we distinguish between these cases by using the superscript LD (lower dimension). We align the corresponding sets for the Case χ_{179} in the Appendix C. In this paper, we do not consider the T and μ dependence of the parameters.

For the sake of the comparison between the dimensional and three momentum cutoff regularizations, we also show the sets of parameters in the Case Cutoff,

Case Cutoff $m_\pi, m_{\rm K}, f_\pi, m_{\eta'}$.

In Table IV, we display the values of parameters for various m_u. It is to be noted that in the cutoff regularization, the six parameters, m_u, $m_d(=m_u)$, m_s, G, K and cutoff scale Λ, are fixed by using the four physical observables (12) and choosing several values of m_u.

III. CONSTITUENT QUARK MASSES

Before going through the meson properties, let us discuss the results for the constituent quark masses m_i^*. This is important because the constituent quark masses determine the scale of the system, and they play a crucial role

in the studies of the transition temperature and chemical potential.

A. m^* in the DR scheme

In Fig. 1, we display the numerical results for the constituent quark masses which are obtained by solving the gap equations Eq. (7) as explained in the previous section. We note that the absolute values of m_u^* and m_s^* gradually decrease with increasing temperature, while at low temperature they do not depend on the chemical potential up to its critical value where they suddenly fall. This is a clear signal of the first-order phase transition. It is worth mentioning that the gap equations have three solutions for the constituent quark masses in the first-order phase transition region and stable solutions are realized by the minimum of the thermodynamic potential. Therefore we have numerically analyzed the minimum of the thermodynamic potential in this region, where a finite potential barrier causes the first-order phase transition.

Similar pictures correspond to the different values of m_u as is shown in Fig. 2 where the dependence of m_u^* on T and μ is given in the Case m_η for fixed values of $m_u = 3$, 4, 5, 5.5 and 6 MeV. These pictures again indicate the crossover transition for low μ and the first-order phase transition for low T. Thus the behavior of the first-order and crossover transitions holds for the different values of m_u in the Case m_η.

In Fig. 3 there are shown m_s^* for different values of m_u as the functions of T or μ in the Case m_η. We see that $|m_s^*|$ as a function of T (at fixed low μ) decreases continuously in Fig. 3(a). On the other hand, there appear two discontinuities in the μ dependence at low T (see Fig. 3(b)). The first discontinuity is particularly important because the corresponding discontinuity in the μ dependence of m_u^* is large as seen in Fig. 2(b). These gaps manifest the effect of approximate $\mathrm{SU_L}(2) \otimes \mathrm{SU_R}(2)$ restoration. The gap seen

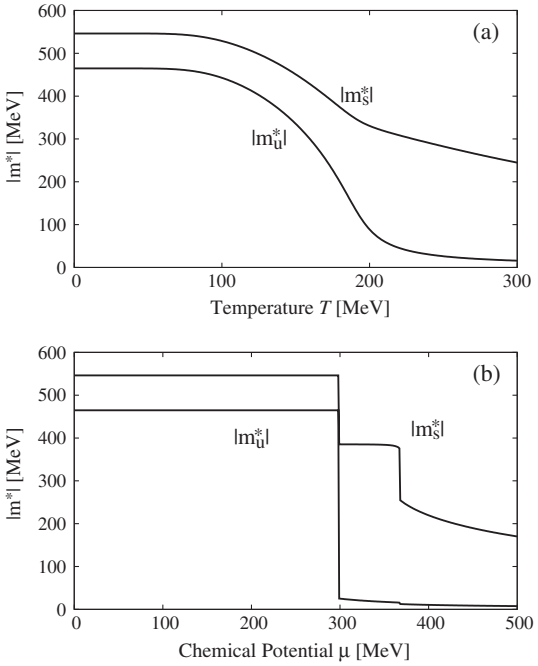

FIG. 1. m_i^* in the Case m_η^{LD} with $m_u = 3$ MeV. (a) finite T and $\mu = 0$; (b) finite μ and $T = 10$ MeV.

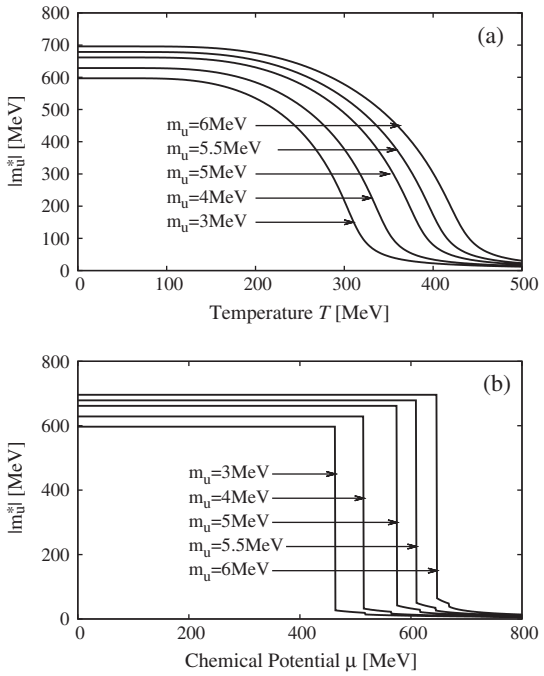

FIG. 2. m_u^* in the Case m_η with various m_u. (a) finite T and $\mu = 0$; (b) finite μ and $T = 10$ MeV.

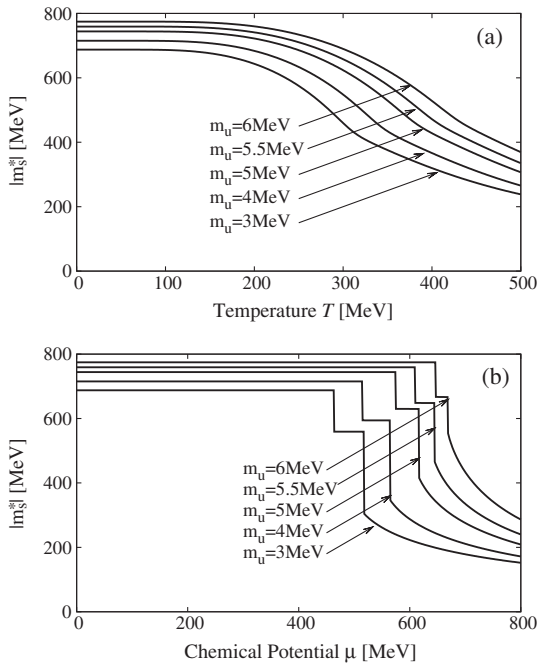

FIG. 3. m_s^* in the Case m_η with various m_u. (a) finite T and $\mu = 0$; (b) finite μ and $T = 10$ MeV.

TABLE V. Constituent quark mass m_u^* [MeV].

m_u	Case m_η^{LD}	Case m_η	Case χ_{170}	Case χ_{179}	Case χ_{179}^{HD}
3.0	−467	−597	−453	−455	−1942
4.0	−460	−623	−439	−442	−2260
5.0	−453	−662	−423	−427	−
5.5	−	−679	−415	−420	−
6.0	−	−696	−408	−412	−

in m_s^* (Fig. 3(b)) is considerably smaller compared to that of m_u^*, since according Eq. (7), due to the large contribution of m_s, the absolute value of m_s^* is larger than that of m_u^*. The second discontinuity comes from the effect of the partial $\mathrm{SU_L}(3) \otimes \mathrm{SU_R}(3)$ restoration. Even after the partial restoration takes place, $|m_s^*|$ is still heavy, $m_s^* \sim \mathcal{O}(100)$ MeV, since the chiral symmetry involving the strange quark is badly broken. Then we define the phase transition through only considering the change of ϕ_u in the following section (Sec. V). We noted that the critical chemical potential is less than the constituent quark mass at $T = 0$ in the DR for $2 \leq D < 3$ at the chiral limit [9].

Other three parameter sets, namely, Cases χ_{170}, χ_{179}, and χ_{179}^{HD}, lead qualitatively to similar results. However, it is worth mentioning that the Case χ_{179}^{HD}, although reproduces proper values for the meson properties discussed in [13], shows quite different quantitative behavior. The constituent quark masses are one order of magnitude larger than the ones in the other parameter sets. This leads to unphysical results for the chiral phase transition; the transition temperature becomes of the order of 1 GeV which is much larger than the physically expected value. This may indicate that the parameters of the Case χ_{179}^{HD} are not suitable to describe the chiral dynamics in this model. To explicitly compare these parameter sets, we align the numerical results for the constituent quark mass, m_u^*, in Table V. There one can clearly see that the values in the Case χ_{179}^{HD} are considerably larger than the ones in the other parameter sets. Since the model predictions in the Cases χ_{170} and χ_{179} are almost the same due to the similar values of m_u^* and the model parameters, we shall only show the results in the Case χ_{170}. In what follows, therefore, we will focus on the Cases m_η^{LD}, m_η, and χ_{170}.

B. m^* in the cutoff regularization scheme

Here we present the results obtained in the widely used sharp-cutoff scheme to make comparisons with our results of the DR.

The numerical results for the constituent quark masses m_u^* and m_s^* for the case $m_u = 5.5$ MeV are shown in Fig. 4. It is found that the T and μ dependencies are similar to the DR case. Figure 5 shows qualitative difference between the cases of $m_u = 5.5$ MeV, and, $m_u = 3$, 4, 5 MeV. The μ dependence of the constituent quark mass m_u^* has discontinuity in the case of $m_u = 5.5$ MeV, while m_u^* decreases

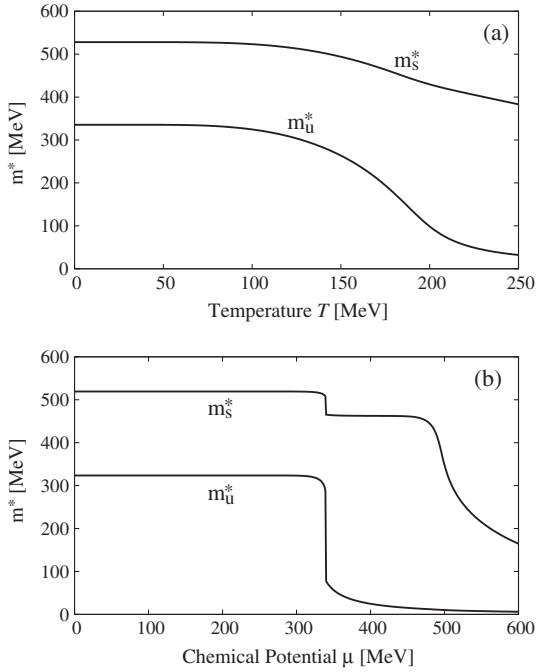

FIG. 4. m_u^* and m_s^* in the case of cutoff for $m_u = 5.5$ MeV. (a) finite T and $\mu = 0$; (b) finite μ and $T = 10$ MeV.

continuously in the cases of $m_u = 3$, 4, 5 MeV. Thus, we have the phase transition of the first order in the case of $m_u = 5.5$ MeV and crossover in the other cases. This is a critical qualitative difference between the dimensional and cutoff regularizations.

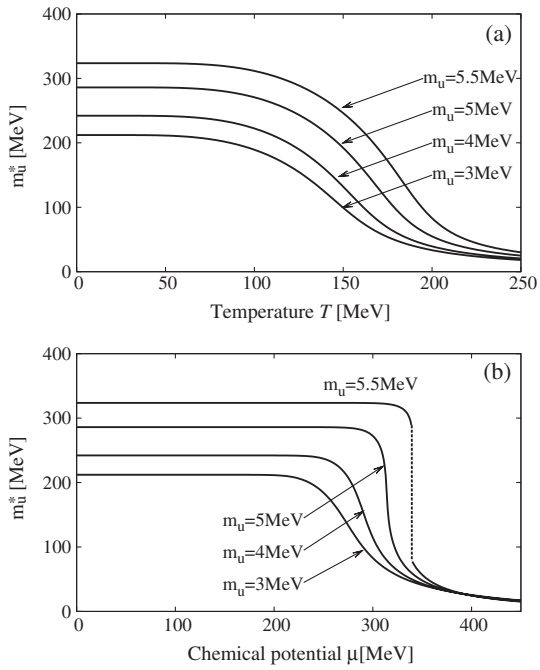

FIG. 5. m_u^* in the case of cutoff. (a) finite T and $\mu = 0$; (b) finite μ and $T = 10$ MeV.

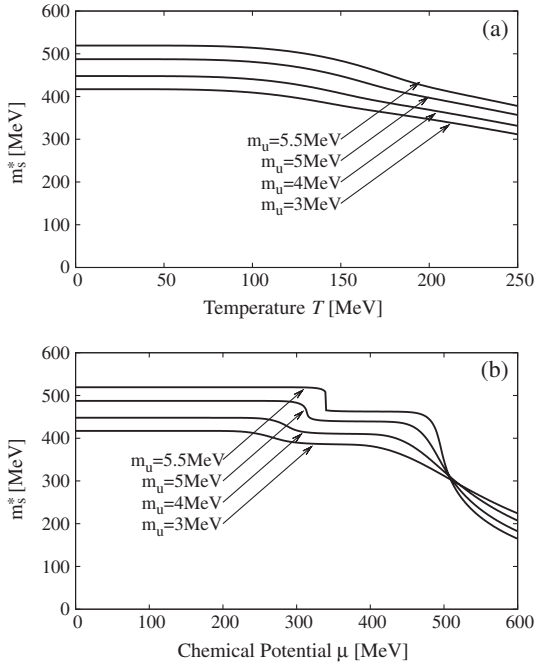

FIG. 6. m_s^* in the case of cutoff. (a) finite T and $\mu = 0$; (b) finite μ and $T = 10$ MeV.

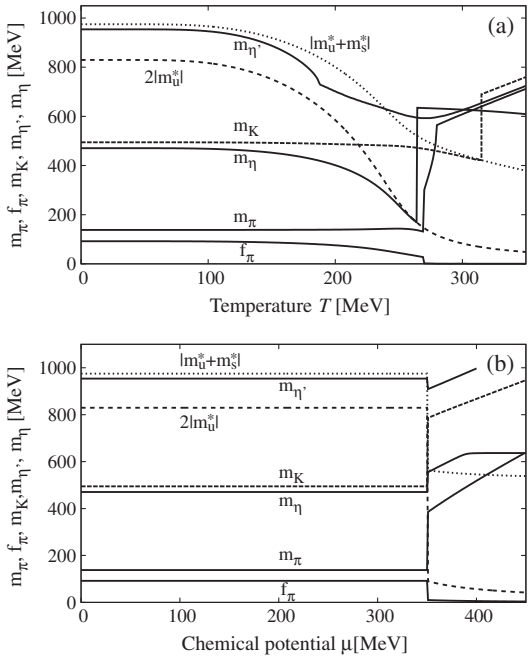

FIG. 7. Case χ_{170} with $m_u = 5.5$ MeV. (a) finite T and $\mu = 0$; (b) finite μ and $T = 10$ MeV.

Figure 6 displays the corresponding results for m_s^*. Note that the T dependence of m_s^* resembles those in the two regularizations, which is seen in Figs. 3(a) and 6(a). However, as seen from Figs. 3(b) and 6(b), the μ dependence of m_s^* is different. The chemical potential dependence in the cutoff regularization are smoother than those in the DR case.

IV. MESON PROPERTIES

In this section, we will show the meson properties, $\{m_\pi, f_\pi, m_{\rm K}, m_\eta, m_{\eta'}\}$, in the two regularizations. We present the Cases m_η and χ_{170} with $m_u = 5.5$ MeV, and $m_\eta^{\rm LD}$ with $m_u = 3$ MeV. The reason of these choices is that the case with $m_u = 5.5$ MeV is a frequently used value in the cutoff regularization [6,18]. As the Case $m_\eta^{\rm LD}$ does not have solutions at $m_u = 5.5$ MeV, we select the $m_u = 3$ MeV case in which the critical temperature of the chiral phase transition is close to empirical data (see Sec. V).

A. Meson properties in DR

Here the numerical results of the meson properties are presented for the Cases χ_{170}, m_η and $m_\eta^{\rm LD}$ with some discussion on their behavior.

Figure 7 shows the results of the meson properties for (a) finite T and $\mu = 0$, and (b) finite μ and $T = 10$ MeV in the Case χ_{170} with $m_u = 5.5$ MeV. As one can observe from the upper panel, m_π and m_η stay almost constant until they cross $2|m_u^*|$, then suddenly jump. In the similar manner, $m_{\rm K}$ is nearly constant below the value $|m_u^* + m_s^*|$, and it enhances when $m_{\rm K}$ becomes $|m_u^* + m_s^*|$. f_π decreases monotonously and becomes negligibly small after m_π exceeds $2|m_u^*|$. At low T the dependence of meson properties on μ has sharp discontinuities as seen in Fig. 7(b), where the masses m_π, $m_{\rm K}$, m_η suddenly get larger and $m_{\eta'}$, f_π falls off. These sharp discontinuities come from the discontinuous change of the chiral condensate, which corresponds to the strong first-order phase transition. On the other hand in the upper panel the meson masses also show jumps as functions of T, although the chiral condensates change continuously with T. This comes from the singular behavior which appears particularly in the lower dimensions $D < 4$. Below, we will discuss the origin of these discontinuities through the analysis of the solution for the pion state.

In Fig. 8 the function $\mathcal{F}_\pi(k^0) = {\rm Re}[1 - 2K_3\Pi_\pi(k^0)]$ is plotted which determines the pion mass through the

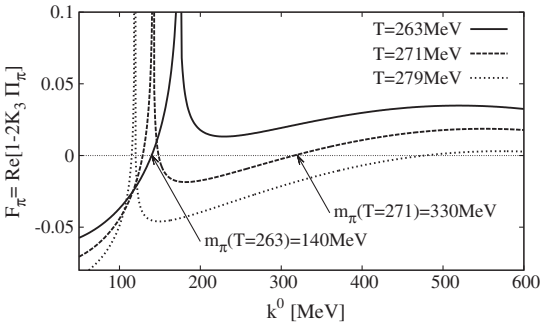

FIG. 8. $\mathcal{F}_\pi$ (denominator of Δ_π) for three fixed values of T, 263, 271, 279 MeV, in the Case χ_{170} with $m_u = 5.5$ MeV at $\mu = 0$.

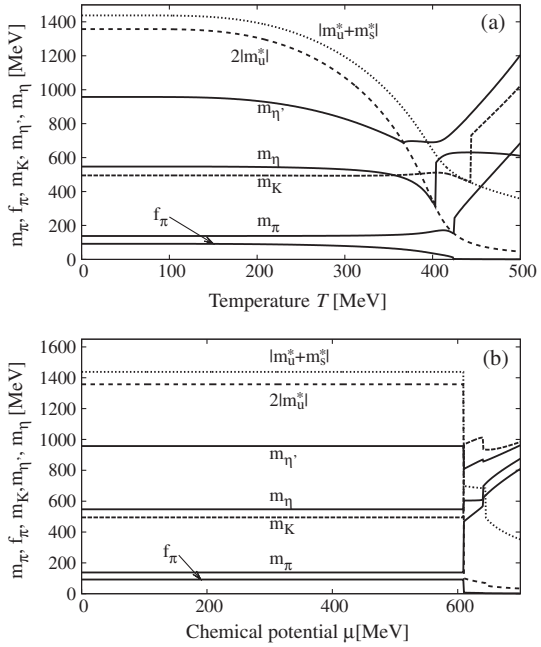

FIG. 9. Case m_η with $m_u = 5.5$ MeV. (a) finite T and $\mu = 0$; (b) finite μ and $T = 10$ MeV.

condition $\mathcal{F}_\pi(k^0) = 0$ (see Appendix B 1). Note that all the lines diverge at $k^0 = 2|m_u^*|$. Because of this divergent behavior of $\mathcal{F}_\pi(k^0)$, there is a jump in the dependence of the pion mass on T. Namely, we find the unique solution around $k^0 \simeq 140$ MeV at $T = 263$ MeV. However, there appear three candidates for the solution at $T = 271$ MeV; two of them are located near the divergent point and the third is larger. We select the larger value, $k^0 \simeq 330$ MeV, because the pion should acquire a larger mass at high T where the chiral symmetry is expected to be restored. This is the reason why the discontinuous change of m_π at some T, is not originated from the sudden change of the chiral condensate ϕ_u. In Appendix B 1, we give the technical details on the divergence in $\mathcal{F}_\pi$.

In Figs. 9 and 10, we show the results for the Case m_η and $m_\eta^{\rm LD}$. We observe the similar pictures in these two cases; smooth dependence on T at zero μ, and similar discontinuities in the dependence on μ at low T. As is seen in Figs. 9(b) and 10(b), there are two discontinuities. The first discontinuity comes from the effect of the gap for m_u^*, and the second discontinuity comes from the one for m_s^*. These gaps are confirmed in Figs. 2(b) and 3(b).

We have also calculated meson properties for the cases of different m_u, and found that the differences between various cases are rather nominal, therefore we showed the results for the case of a particular m_u.

B. Meson properties in cutoff regularization

Here we present the results for the meson properties in the cutoff case.

Figure 11 shows the dependence of the meson properties on T and μ. The results in the two regularizations look similar to each other. The most noticeable difference is that the curves are rather smooth in the cutoff case. There are no discontinuities for low μ in Fig. 11(a), because Eq. (B11) does not include divergence for $D = 4$, and the solution on the real axis survives in the high-temperature region. In the

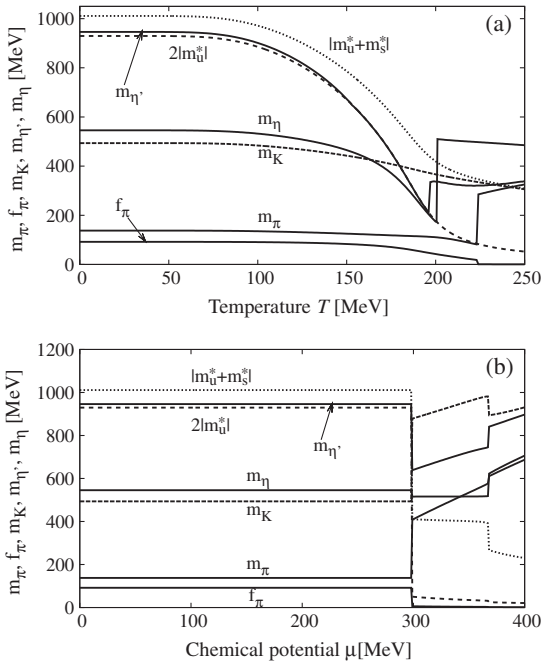

FIG. 10. Case $m_\eta^{\rm LD}$ with $m_u = 3$ MeV. (a) finite T and $\mu = 0$; (b) finite μ and $T = 10$ MeV.

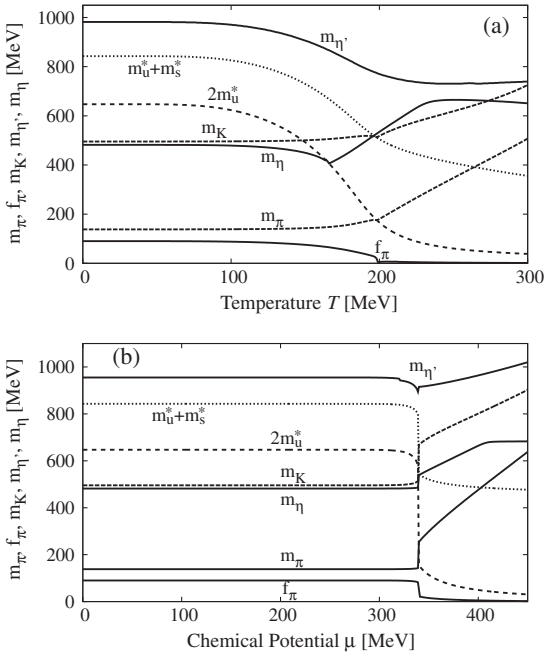

FIG. 11. Meson properties in the case of cutoff for $m_u = 5.5$ MeV. (a) finite T and $\mu = 0$; (b) finite μ and $T = 10$ MeV.

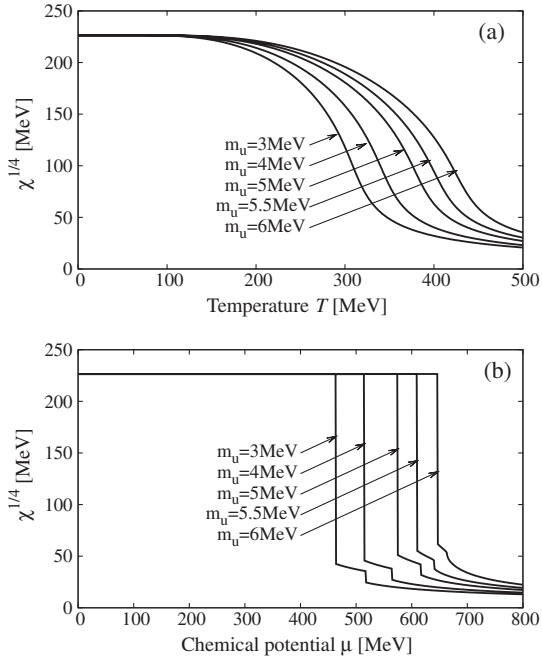

FIG. 12. Case m_η: Topological susceptibility $\chi^{1/4}$. (a) finite T and $\mu = 0$; (b) finite μ and $T = 10$ MeV.

high-T region, the behavior of m_η (soft mode) becomes flat. This tendency is also seen in [16], and in Figs. 7(a), 9(a), and 10(a). On the other hand, m_η increases linearly at high T in [18]. The difference may come from the definitions of m_η, i.e., we and [16] define m_η in the real part of the inverted propagator and [18] treats it in the complex plane of the momentum. In the high-T region, a

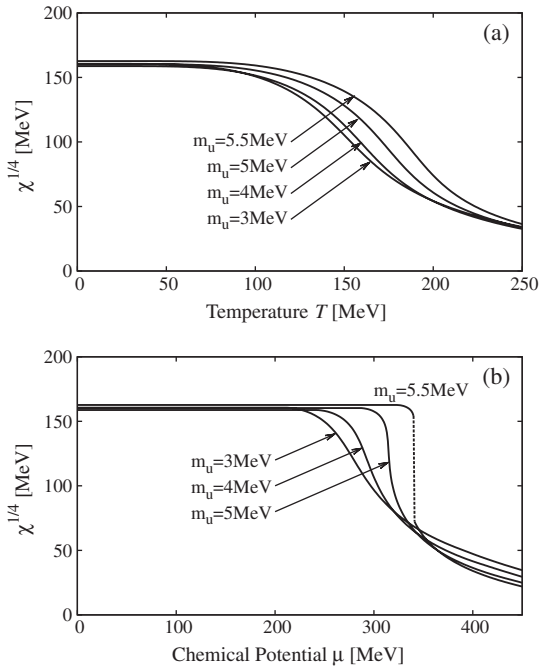

FIG. 13. Topological susceptibility in the case of cutoff. (a) finite T and $\mu = 0$; (b) finite μ and $T = 10$ MeV.

contribution from the imaginary part of the inverse propagator may become important in these cases. In Fig. 11(b) the gap at $\mu \simeq 340$ MeV is smaller than the gap of the DR case. This can be understood from the fact that the gap of m_u^* in the cutoff scheme is smaller than the one in the DR scheme (see Figs. 2(b) and 5(b)).

C. Results of topological susceptibility

As mentioned above, the topological susceptibility χ is an important quantity, because it is intimately related to the chiral and $U_A(1)$ symmetry of QCD.

Figures 12 and 13 display the curves for the topological susceptibility χ [shown in Eq. (11)] as the functions of T or μ which resemble the curves for m_u^* in Figs. 2 and 5, respectively. Thus we confirm that the topological susceptibility is influenced indeed by the chiral symmetry breaking.

V. CRITICAL TEMPERATURE

We have seen that the chiral condensate and the topological susceptibility always show discontinuous changes at low temperature in the DR, which indicates the first-order phase transition. The tendency remains in all cases with different parameter sets. On the other hand, the order of transition is different for the different parameter sets in the cutoff case as confirmed in Fig. 5(b) and 13(b). This may indicate that the transition pattern crucially depends on the regularization procedures. Therefore it is interesting to study the values of the critical temperature T_c for various cases both in dimensional and cutoff regularizations. Here we focus on T_c at $\mu = 0$, and make the comparison among the two regularization and the lattice QCD simulations.

There are several ways to define the critical temperatures. In this paper, we shall employ the definition given by the maxima of

$$\frac{\partial \phi_u}{\partial T}. \tag{13}$$

In Table VI the numerical results for the critical temperature are aligned for various parameter sets. In the Case m_η^{LD} with $m_u = 4$ and 5 MeV, we can not find a physically meaningful behavior for the phase transition; the absolute value of m_u^* becomes larger with increasing T. That is why these cases are marked by ''none'' in the table.

Note that the values of T_c in the DR except for the Case m_η^{LD} are larger than ones in the cutoff case. The Case m_η^{LD}

TABLE VI. Critical temperature T_c.

m_u	m_η^{LD}	m_η	χ_{170}	Cutoff
3.0	184	304	253	146
4.0	none	336	249	155
5.0	none	374	243	170
5.5	–	395	240	184
6.0	–	419	237	–

at $m_u = 3$ MeV leads almost to the same value of T_c as in the cutoff case at $m_u = 5.5$ MeV which is comparable with the result in the lattice QCD simulation, 150–200 MeV [19]. We see that T_c becomes larger with increasing m_u in the Case m_η while T_c does not change drastically with m_u in the Case χ_{170}. This can be explained by the values of m_u^*.

VI. SUMMARY AND DISCUSSIONS

In this paper we studied the nonet meson characteristics, m_π, f_π, m_{K}, m_η, $m_{\eta'}$, and χ at finite temperature and chemical potential in the NJL model with DR. Many of meson properties show reasonable behavior, which is similar to one obtained in the model with the cutoff regularization.

We examined the behavior of the constituent quark masses, m_u^* and m_s^*, in the two regularizations. T dependence of the constituent quark masses at low μ does not depend essentially on the way of regularization. However, μ dependence of the constituent quark masses at low T depends on the regularization way around the critical chemical potential. In the DR, the phase transition at low T is always of the first order for various choices of m_u. This tendency is consistent with the current consensus about the transition to be of the first order in the chiral limit [20]. On the other hand in the cutoff case, the gap at the critical chemical potential becomes smaller with decreasing value of m_u, and it eventually vanishes resulting in crossover transition (see Fig. 5). This happens due to the fact that the larger cutoff Λ diminishes the coupling strength which leads to the smoother change of the order parameters. Decreasing the coupling strength weakens nonperturbative effects. This explains the effect of the UV-cutoff which is also seen in the work [21] as the effect of the cutoff in the temporal direction.

Using the obtained values of the constituent quark masses, we evaluated meson properties at finite T and/or μ in the two regularizations. T dependence of the meson masses at low μ are similar to each other except around $m_{\mathrm{P}} \simeq |m_i^* + m_j^*|$. Since the singularity of the pion self-energy $\Pi_{\mathrm{P}}(k^2)$ appears at $k^2 = (m_i^* + m_j^*)^2$ for $D < 4$, the behavior of meson masses becomes discontinuous in the DR. μ dependence of the meson masses at low T also does not essentially depend on the way of regularization except at the region of the critical chemical potential. Since the gap of m_u^* in the DR case is larger than one in the cutoff case, the gap of the meson mass becomes large. As is known, there is an uncertainly in the definition of the meson masses due to an unphysical imaginary part [7]. Here we discard the imaginary part by hand to evaluate the meson masses. The behavior of f_π as the functions of T or μ in the DR case resembles one in the cutoff case. We also evaluated the topological susceptibility χ as the functions of T or μ in the two regularizations. The behavior of χ is similar to one of m_u^*.

In the DR, we examined the three parameter set cases: χ_{170}, m_η, and m_η^{LD}. Parameters of each set are fixed by fitting physical quantities at T, $\mu = 0$ [13]. Most of the properties concerning meson masses and decay constants are similar to each other in the three cases. However, the large difference is seen in the values of the critical temperature and of the critical chemical potential. One of the sources of this difference may be the strength of couplings, i.e., increasing the values of the coupling strength decreases the values of the critical temperature and the critical chemical potential. We actually calculated the critical temperature, T_c. In the Case m_η^{LD} at $m_u = 3$ MeV, the critical temperature is almost the same as in the cutoff case at $m_u = 5.5$ MeV which is comparable to the result in the lattice QCD simulation.

The lessons we learned in this paper are twofold: (i) similarities in the predicted meson properties and (ii) remarkable differences seen in the order of the chiral phase transition at finite chemical potential. Regarding the point (i) we have been convinced that the NJL model predictions do not depend drastically on whether one uses the dimensional or cutoff regularization procedure. This may be the regularization independent aspect of the NJL model, which is an intriguing problem to be studied in more detail in future. As to the point (ii) the results of the paper suggest that the critical point in the phase diagram on $T - \mu$ plane shows different behavior. We think that it is interesting to study the behavior of the chiral phase transition and the phase diagrams of the model in more detail, especially in context of how the location of the critical point depends on the parameters in the different regularization schemes.

ACKNOWLEDGMENTS

H. K. is supported by the Grant No. NSC-99-2811-M-033-017 from National Science Council (NSC) of Taiwan.

APPENDIX A: CHIRAL CONDENSATE

By taking the trace with respect to the Dirac spinor indices in Eq. (8), we get the chiral condensate

$$\phi_i = \mathrm{tr1} \cdot m_i^* \int \frac{d^{D-1}p}{(2\pi)^{D-1}} T \sum_{n=-\infty}^{\infty} \frac{-1}{\omega_n^2 + E_i^2}, \tag{A1}$$

where $\mathrm{tr1} = N_c \cdot 2^{D/2}$. After performing the frequency summation, we arrive at the expression

$$\phi_i = \mathrm{tr1} \cdot m_i^* \int \frac{d^{D-1}p}{(2\pi)^{D-1}} \frac{-1}{2E_i} \left[1 - \sum_{\pm} f(E_i^{\pm}) \right], \tag{A2}$$

with the Fermi-Dirac distribution $f(E)$ given by

$$f(E_i^{\pm}) \equiv \frac{1}{1 + e^{\beta E_i^{\pm}}}. \tag{A3}$$

APPENDIX B: MESON PROPERTIES

Here we evaluate meson masses, decay constants, and topological susceptibility. More detailed, self-contained calculations are presented in the review paper [5].

1. π and K masses

Meson masses are obtained through examining the pole structure of their propagators. Using the random-phase approximation and the $1/N_c$ expansion, we get the meson propagators of the form [5,6]

$$\Delta_{\mathrm{P}}(k^2) = \frac{2K_\alpha}{1 - 2K_\alpha \Pi_{\mathrm{P}}(k^2)} + \mathrm{O}(N_c^{-1}), \tag{B1}$$

where the index P$(= \pi, \mathrm{K})$ denotes the meson species and α labels the isospin channel. The pole position is determined by the equation

$$1 - 2K_\alpha \Pi_{\mathrm{P}}(x^2) = 0, \tag{B2}$$

where x^2 is regarded as the square of a meson mass, i.e., m_π^2 or m_{K}^2.

The effective couplings, K_α, of mesons become

$$K_3 \equiv G - \frac{1}{2}K\phi_s, \quad \text{for } \pi^0, \tag{B3}$$

$$K_6 \equiv G - \frac{1}{2}K\phi_u, \quad \text{for } \mathrm{K}^0, \bar{\mathrm{K}}^0. \tag{B4}$$

The self-energy, Π_{P}, of the propagator is given by

$$\Pi_{\mathrm{P}}(k^2)\delta_{\alpha\beta} = \int \frac{d^D p}{i(2\pi)^D} \mathrm{tr}[\gamma_5 T_\alpha S^i(p + k/2)\gamma_5 T_\beta^\dagger S^j(p - k/2)], \tag{B5}$$

where the trace runs over flavor, spinor, and color indices. The flavor $SU(3)$ matrices T_α are $T_3 = \lambda_3$ for π^0, $T_6 = (\lambda_6 + i\lambda_7)/\sqrt{2}$ for K^0, and $T_6^\dagger$ for $\bar{\mathrm{K}}^0$. Then the self-energy for π^0, K^0 and $\bar{\mathrm{K}}^0$ can be written as

$$\Pi_\pi(k^2 = m_\pi^2) = 2\Pi_5^{uu}(k^2 = m_\pi^2), \tag{B6}$$

$$\Pi_{\mathrm{K}}(k^2 = m_{\mathrm{K}}^2) = 2\Pi_5^{su}(k^2 = m_{\mathrm{K}}^2), \tag{B7}$$

where $\Pi_5^{ij}(k^2)$ is defined by

$$\Pi_5^{ij}(k^2) = \int \frac{d^D p}{i(2\pi)^D} \mathrm{tr}[\gamma_5 S^i(p + k/2)\gamma_5 S^j(p - k/2)] = -\frac{1}{2}\left(\frac{\phi_i}{m_i^*} + \frac{\phi_j}{m_j^*}\right) + \frac{1}{2}[k^2 - (m_i^* - m_j^*)^2]I_{ij}, \tag{B8}$$

with

$$I_{ij} = \int \frac{d^D p}{i(2\pi)^D} \frac{\mathrm{tr}1}{(p^2 - m_i^{*2})[(p - k)^2 - m_j^{*2}]}. \tag{B9}$$

The integral above becomes

$$I_{ij} = \int \frac{d^{D-1} p}{i(2\pi)^{D-1}} \frac{\mathrm{tr}1}{D_{ij}^+} \left\{ \sum_{i \leftrightarrow j} \frac{1}{2E_i} \left[1 - \sum_{s=\pm} \frac{S_{ji}}{D_{ij}^-} f(E_i^s) \right] - \frac{k_0}{D_{ij}^-}[f(E_i^+) - f(E_i^-) - f(E_j^+) + f(E_j^-)] \right\} \tag{B10}$$

where $D_{ij}^\pm = (E_i \pm E_j)^2 - k^2$ and $S_{ij} = m_i^{*2} - m_j^{*2} - k^2$. In practice we first solve the gap equations to get the chiral condensates ϕ_i and constituent quark masses m_i^*, then we scan the solution of Eq. (B2) in evaluating m_π and m_{K}. In the actual numerical calculations, we choose the rest frame $k^\mu = (k^0, \mathbf{0})$.

It should be noted that I_{ij} as a function of k^0 ($\mathbf{k} = \mathbf{0}$) has a singularity. Since the pion self-energy Π_π consists of the function I_{uu}, it is divergent at the singularity. $\Pi_\pi(k^2)$ has a cut in the region $k^0 \geq 2|m_u^*|$ on the real axis. One should move to the other Riemann sheet to calculate $\Pi_\pi(k^2)$ at the cut. The vacuum part $I_{uu}^{(v)}$ is written as

$$I_{uu}^{(v)} = \frac{N_c}{(2\pi)^{D/2}} \Gamma\left(2 - \frac{D}{2}\right) \int_0^1 dx L_{uu}^{D/2-2}(k^2), \tag{B11}$$

where

$$L_{uu}(k^2) = m_u^{*2} - k^2 x(1 - x). \tag{B12}$$

The function $I_{uu}(k^2)$ is divergent at $k^2 = 4m_u^{*2}$ for $D < 4$. Then $\Pi_\pi(k^2)$ has the singularity at $k^0 = 2|m_u^*|$ which is confirmed in Fig. 8 where $D = 2.47$ (Case χ_{170} with $m_u = 5.5$ MeV). The divergence appears at the resonance position. It does not mean the existence of a bound state except for $k^0 = 2|m_u^*|$. In Fig. 8 three solutions are observed for $\mathcal{F}_\pi = 0$ at $T = 271$ and 279 MeV. Two of the solutions are located near the singularity at $k^0 = 2|m_u^*|$. We take the solution with the larger k^0 to express the pion mass. Thus the meson masses jump as functions of T near the critical temperature.

As is shown in Fig. 8, the larger solution disappears for $T \gtrsim 279$ MeV. In this case we determine the meson mass as k^0 at the minimum of $|\mathcal{F}_\pi|$. On the contrary, the reliable solution always exists and the smaller two solutions are degenerate above the critical chemical potential at $T = 10$ MeV.

2. π and K decay constants

Here, we display the equations determining f_{P}, the pion and kaon decay constants, with P$(= \pi, \mathrm{K})$.

$$ik_\mu f_{\mathrm{P}}\delta_{\alpha\beta} = -M_0^{4-D} \int \frac{d^D p}{(2\pi)^D} \mathrm{tr}\left[\gamma_\mu \gamma_5 \frac{T_\alpha}{2} S^i g_{\mathrm{P}qq}(0) \gamma_5 T_\beta^\dagger S^j \right], \tag{B13}$$

where the renormalization scale M_0 is introduced so that the decay constant has a correct mass dimension,

$\dim(f_{\rm P}) = 1$. The trace is with respect to the flavor, spinor, and color indices. The meson-to-quark-quark coupling, $g_{{\rm P}qq}$, is defined by

$$g_{{\rm P}qq}(k^2)^{-2} = M_0^{4-D}\frac{\partial \Pi_{\rm P}(k^2)}{\partial k^2}. \tag{B14}$$

Equation (B13) can be rewritten in the following form:

$$f_{\rm P}^2 = -M_0^{4-D} g_{{\rm P}qq}^2 I_{\rm P}^2/k^2, \tag{B15}$$

where $I_\pi = m_u^* I_{uu}(k^2)k_\mu$ and

$$I_{\rm K} = {\rm tr1}\int \frac{d^D p}{i(2\pi)^D}\frac{(m_s^* - m_u^*)p_\mu - m_s^* k_\mu}{(p^2 - m_s^{*2})[(p-k)^2 - m_u^{*2}]}.$$

By inserting the values of the constituent quark masses m_i^* and the renormalization scale M_0, one can easily evaluate the decay constants.

3. η and η' mesons

The equation which determines η meson masses becomes a 2×2 matrix due to the well known $\mathrm{U_A(1)}$ anomaly. In the leading order of the $1/N_c$ expansion, the propagator of the $\eta - \eta'$ system becomes

$$\mathbf{\Delta}^+(k^2) = 2\mathbf{K}^+[1 - 2\mathbf{K}^+\mathbf{\Pi}(k^2)]^{-1}, \tag{B16}$$

where $\mathbf{K}^+$ and $\mathbf{\Pi}$ are given by

$$\mathbf{K}^+ = \begin{pmatrix} K_{00} & K_{08} \\ K_{80} & K_{88}\end{pmatrix}, \tag{B17}$$

$$\mathbf{\Pi} = \begin{pmatrix} \Pi_{00} & \Pi_{08} \\ \Pi_{80} & \Pi_{88}\end{pmatrix}, \tag{B18}$$

with

$$K_{00} = G + \frac{1}{3}K(\phi_s + 2\phi_u), \tag{B19}$$

$$K_{88} = G + \frac{1}{6}K(\phi_s - 4\phi_u), \tag{B20}$$

$$K_{08} = K_{80} = \frac{\sqrt{2}}{6}K(\phi_s - \phi_u), \tag{B21}$$

and

$$\Pi_{00}(k^2) = \frac{2}{3}[2\Pi_5^{uu}(k^2) + \Pi_5^{ss}(k^2)], \tag{B22}$$

$$\Pi_{88}(k^2) = \frac{2}{3}[\Pi_5^{uu}(k^2) + 2\Pi_5^{ss}(k^2)], \tag{B23}$$

$$\Pi_{08}(k^2) = \Pi_{80}(k^2) = \frac{2\sqrt{2}}{3}[\Pi_5^{uu}(k^2) - \Pi_5^{ss}(k^2)]. \tag{B24}$$

The condition which determines the η and η' masses is

$$\det[1 - 2\mathbf{K}^+\mathbf{\Pi}(x^2)] = 0. \tag{B25}$$

Furthermore, the left-hand side of the above equation can be factorized by the following quantities:

$$\mathcal{F}_\eta(k^2) = A + C - \sqrt{(A-C)^2 + 4B^2}, \tag{B26}$$

$$\mathcal{F}_{\eta'}(k^2) = A + C + \sqrt{(A-C)^2 + 4B^2}, \tag{B27}$$

with

$$A(k^2) = K_{88} - 2\Pi_{00}(k^2)\det\mathbf{K}^+,$$
$$B(k^2) = -K_{08} - 2\Pi_{08}(k^2)\det\mathbf{K}^+,$$
$$C(k^2) = K_{00} - 2\Pi_{88}(k^2)\det\mathbf{K}^+.$$

We search the mass of η (η') meson via the condition $\mathcal{F}_{\eta(\eta')} = 0$ as discussed in [13].

Using the constituent quark masses derived from the gap equations, we search for the appropriate solutions for m_η and $m_{\eta'}$. The solution for $m_{\eta'}$ on the real axis of k^0 disappears at high T for some parameter sets. In this case we determine the value of $m_{\eta(\eta')}$ at the minimum of $|\mathcal{F}_{\eta(\eta')}|$ as in the pion case.

APPENDIX C: PARAMETER SETS

Here we present the parameter sets obtained in the Case χ_{179} in Tables VII and VIII. As seen in the Case m_η, there exist two sets of parameters, and we distinguish between these cases by using the superscript HD (higher dimension).

TABLE VII. Case χ_{179}.

m_u	m_s	G	K	M_0	D
3.0	78.0	-0.0170	2.70×10^{-7}	120	2.28
4.0	106	-0.0144	2.52×10^{-7}	115	2.36
5.0	136	-0.0120	2.11×10^{-7}	111	2.44
5.5	152	-0.0109	1.90×10^{-7}	110	2.47
6.0	168	$-0.009\,95$	1.70×10^{-7}	108	2.50

TABLE VIII. Case $\chi_{179}^{\rm HD}$.

m_u	m_s	G	K	M_0	D
3.0	74.8	-4.24×10^{-5}	1.38×10^{-13}	2.91	3.22
4.0	100	-6.91×10^{-8}	3.60×10^{-19}	1.15×10^{-25}	3.90

[1] Y. Nambu and G. Jona-Lasinio, Phys. Rev. **122**, 345 (1961); **124**, 246 (1961).
[2] M. Gell-Mann and M. Levy, Nuovo Cimento **16**, 705 (1960).
[3] K. G. Wilson, Phys. Rev. D **10**, 2445 (1974).
[4] U. Vogl and W. Weise, Prog. Part. Nucl. Phys. **27**, 195 (1991).
[5] S. P. Klevansky, Rev. Mod. Phys. **64**, 649 (1992).
[6] T. Hatsuda and T. Kunihiro, Phys. Rep. **247**, 221 (1994).
[7] M. Buballa, Phys. Rep. **407**, 205 (2005).
[8] S. Krewald and K. Nakayama, Ann. Phys. (Leipzig) **216**, 201 (1992).
[9] T. Inagaki, T. Kouno, and T. Muta, Int. J. Mod. Phys. A **10**, 2241 (1995).
[10] R. G. Jafarov and V. E. Rochev, Russ. Phys. J. **49**, 712 (2006).
[11] T. Inagaki, D. Kimura, and A. Kvinikhidze, Phys. Rev. D **77**, 116004 (2008).
[12] T. Fujihara, D. Kimura, T. Inagaki, and A. Kvinikhidze, Phys. Rev. D **79**, 096008 (2009).
[13] T. Inagaki, D. Kimura, H. Kohyama, and A. Kvinikhidze, Phys. Rev. D **83**, 034005 (2011).
[14] M. Kobayashi and T. Maskawa, Prog. Theor. Phys. **44**, 1422 (1970); M. Kobayashi, H. Kondo, and T. Maskawa, Prog. Theor. Phys. **45**, 1955 (1971).
[15] G.'t Hooft, Phys. Rev. D **14**, 3432 (1976); **18**, 2199(E) (1978); Phys. Rep. **142**, 357 (1986).
[16] K. Fukushima, K. Ohnishi, and K. Ohta, Phys. Rev. C **63**, 045203 (2001).
[17] C. Amsler *et al.* (Particle Data Group), Phys. Lett. B **667**, 1 (2008), and 2009 partial update for the 2010 edition.
[18] P. Rehberg, S. P. Klevansky, and J. Hufner, Phys. Rev. C **53**, 410 (1996).
[19] For a review, K. Fukushima and T. Hatsuda, Rep. Prog. Phys. **74**, 014001 (2011).
[20] R. D. Pisarski and F. Wilczek, Phys. Rev. D **29**, 338 (1984).
[21] J. W. Chen, K. Fukushima, H. Kohyama, K. Ohnishi, and U. Raha, Phys. Rev. D **81**, 071501 (2010).